

ORIGINAL ARTICLE

Effect of high-pressure detonation products on fuel injection and propagation characteristics of detonation wave



Gaoyang Ge^a, Li Deng^b, Hu Ma^{a,*}, Zhenjuan Xia^a, Xiao Liu^c, Changsheng Zhou^a

^aSchool of Mechanical Engineering, Nanjing University of Science and Technology, Nanjing, Jiangsu, 210094, China

^bInstitute of Chemical Materials, China Academy of Engineering Physics, Mianyang, Sichuan, 621999, China

^cCollege of Power and Energy Engineering, Harbin Engineering University, Harbin, Heilongjiang, 150001, China

Received 30 November 2020; accepted 13 December 2021

Available online 16 March 2022

KEYWORDS

High-pressure detonation products;
Ion voltage;
Feedback;
Purgation;
Long-duration test;
Low frequency oscillation

Abstract The effect of high-pressure detonation products on fuel injection and propagation characteristics of detonation wave has been investigated in the form of ion voltage by varying the equivalence ratio (*ER*), air mass flux, and operation duration with hydrogen-air mixtures. It has been shown experimentally that the ion voltage decays gradually during the initial stage of rotating detonation wave (RDW). The attenuation of ion voltage is a general phenomenon, and the decay rate of ion voltage and its peak value of the trough state are related to the equivalence ratio and air mass flux. The analysis of interaction between the combustor and hydrogen plenum indicates that the feedback of high-pressure detonation products leads to the attenuation of ion voltage. In addition, the long-duration tests show that the ion voltage will recover to a steady state with the extension of reaction time, when the purgation (products leaving plenums) of detonation products is greater than feedback (products entering plenums) of detonation products in the hydrogen plenum. The recovery of ion voltage starts earlier at the higher equivalence ratio and air mass flux, and the peak value of ion voltage in the steady state also increases with

*Corresponding author.

E-mail addresses: gayank@163.com, mahuokok@163.com (Hu Ma).

Peer review under responsibility of Beihang University.



the increase of equivalence ratio and air mass flux. A low frequency oscillation about 10–12 Hz occurs in the RDW at some operation conditions. This low frequency oscillation is related to the interaction between the combustor and hydrogen plenum, and can be eliminated by either increasing the equivalence ratio or decreasing the air mass flux.

© 2022 Beihang University. Publishing services by Elsevier B.V. on behalf of KeAi Communications Co. Ltd. This is an open access article under the CC BY-NC-ND license (<http://creativecommons.org/licenses/by/4.0/>).

1. Introduction

Detonation combustion is a nearly constant-volume process and has the characteristics of high energy-release rate and thermodynamic efficiency [1,2]. As an important application of detonation in propulsion systems, rotating detonation engine (RDE) [3–6] has received increased attention in view of potential benefits compared to conventional combustors operating in deflagration mode. RDE utilizes one or multiple detonation waves propagating in the annular combustor continuously to produce steady thrust. Due to the compact structure, high operating frequency, high thermodynamic efficiency and stable thrust, RDE has the potential to be employed in the future astronautic propulsion.

The development of RDE is particularly rapid in recent years, and significant achievements have been achieved, such as the effects of oxidizer injection slot width [7], reactants mixing effect [8], fuel injection schemes [9], mass flow rate [4,10], operating back pressure [11] and equivalence ratio [12,13] on the regions of existence and wave speed performance of RDW. The propagation stability and operation mode of rotating detonation wave under the subsonic [14] and supersonic [15] injection of the oxidizer are investigated experimentally. The feedback of high-pressure detonation products on the reactant plenums is studied by varying the air injection pressure ratio [16], backpressure [17], injectors [18] and equivalence ratios [19]. In addition, the effect of backpressure on the ignition characteristics and operation modes are investigated by integration of convergent nozzles [20], annular ejector [21], and afterburner [11]. Researchers have revealed that the stability of RDW and the operation map of RDE are closely related to the injection configuration [4,9]. Moreover, the basic operating modes of RDE are also identified as steady single wave [5,8,11], coexistence of single wave and multiple waves [5,12], steady multiple waves [5,11,15], and longitudinal pulsed detonation mode [11,14,16]. Numerical simulations are performed to investigate the effects of spatial non-uniformity of the reactants on the flow features in the detonation combustor [22,23]. The effect of premixed stratification on the wave dynamics of the detonation combustor is studied by premixing part of the fuel into the oxidizer [24].

Due to the high frequency of detonation wave, the flush-mounted high-frequency pressure transducers are

susceptible to be damaged under heavy heat loading and erosion of shock wave, which make it difficult to evaluate the propagation characteristics of RDW during the long-duration test. Therefore, non-contact measurements (optical diagnostic techniques) and durable contact measurement tools are essential for the research of rotating detonation engines. One of them is the ion probe which is widely used in the studies of detonation engines [25,26] and classical detonations [27,28]. The ion concentration in the reaction zone behind the leading shock wave is measured in the form of ion voltage or fluid electrical resistance [26]. The ion probe is reliable to capture the propagation of combustion front. The output value of ion probe can be used to evaluate the propagation characteristics of RDW as well as the interaction between the plenums and combustor during the operation of RDE. In addition, the ion probe removes the false signal detected by PCB sensors caused by non-reacting shock wave [3]. Frolov et al. [15] used a series of ion probes to detect the detonation wave front, and processing of the records by scaling the level of signal in terms of grayscale allows “visualization” of the flow. George et al. [3] applied the ion probes in rotating detonation combustor in the form of fluid electrical resistance to detect the propagation of combustion front. Zdenek [26] developed a pressure sensor based on the ion concentration for long-duration test in PDE, and showed a viable alternative method for measuring pressure.

However, the ion probes are only used to detect the propagation of combustion front in most of studies [15,16,25]. The intensity and variation of ion signals during the test have not attracted much attention. In the paper, the time-dependent ion and pressure signals are acquired with ion probes and piezoelectric transducers during the short-duration test, respectively. The time-dependent pressure signals during the long-duration test are measured by infinite tube pressure (ITP) [21]. The variation of ion concentration during the whole test is investigated in the form of ion voltage. Based on the measured ion signals, the effect of equivalence ratio and air mass flux on the evolution of ion concentration is studied. Moreover, the interaction between the high-pressure detonation products and injection behavior of hydrogen plenum is investigated by analysis of the evolution of ion concentration. The relationship between the purgation of detonation products in the hydrogen plenum and frequency characteristics of RDW is also explored.

2. Experimental setup and measurement techniques

Figure 1 shows the schematic diagram of the RDE test facility, which consists of a model RDE combustor, hydrogen and air delivery system, control system and data acquisition system. The inner diameter, outer diameter and length of the detonation combustor are 70 mm, 80 mm and 40 mm, respectively, resulting in a channel width of 5 mm. A slit-orifice impinging mode is applied to achieve high-quality mixing of hydrogen and air, as shown in **Figure 2(a)**. The air is injected into the combustor through the Laval-nozzle like slit, while the fuel is injected through 90 uniformly distributed orifices along the inner body of RDE. The hydrogen and air mass flow rates are metered upstream of the respective plenums using two sonic nozzles. The global equivalence ratios in all the tests are based on those two values. The detonation in the combustor is initiated using a vertically installed pre-detonator about 8 mm downstream of the injection plane. Hydrogen and oxygen

are injected into the pre-detonator (6 mm diameter, 600 mm long) separately, and the mixture is ignited by a spark when the static pressures in the hydrogen and air plenums reach a steady state. The pre-detonator and combustor are separated by a thin plastic membrane, which is destroyed during each test, to minimize the interaction between the combustor and pre-detonator before ignition.

The instantaneous pressure and ion signals in the annular detonation channel and the time-averaged static pressure in the plenums are applied to study the propagation characteristics and operation mode of rotating detonation wave in the combustor. The position of instrumentation is shown in **Figure 2**. The PCB 113B24 piezoelectric transducers are flush-mounted at the outer body to acquire the time-dependent dynamic pressure fluctuations in the combustor in the short-duration test, while the ITP measurement is used in the long-duration test. The ion probes (I1–I4) are flush-mounted to measure the ion concentration in the reaction zone in the form of voltage. **Tables 1 and 2** show the instrumentations in the short-duration and long-duration tests,

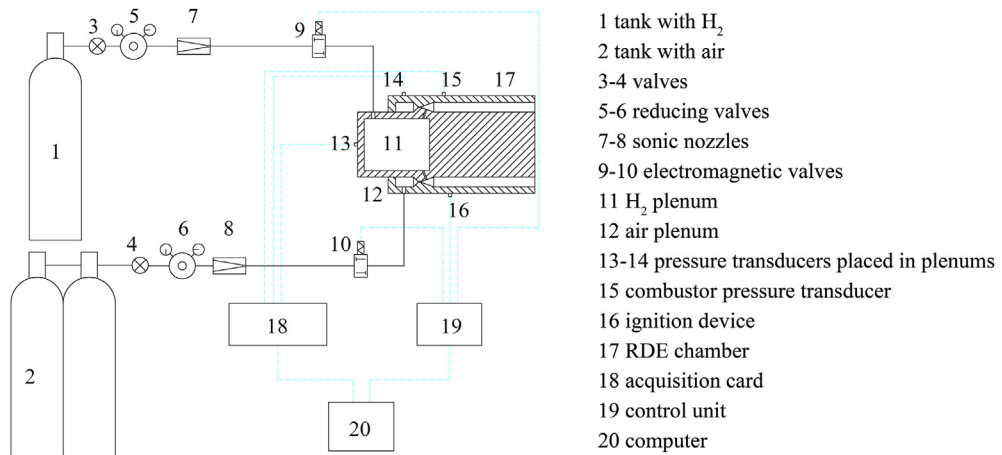


Figure 1 Schematic diagram of the RDE test facility.

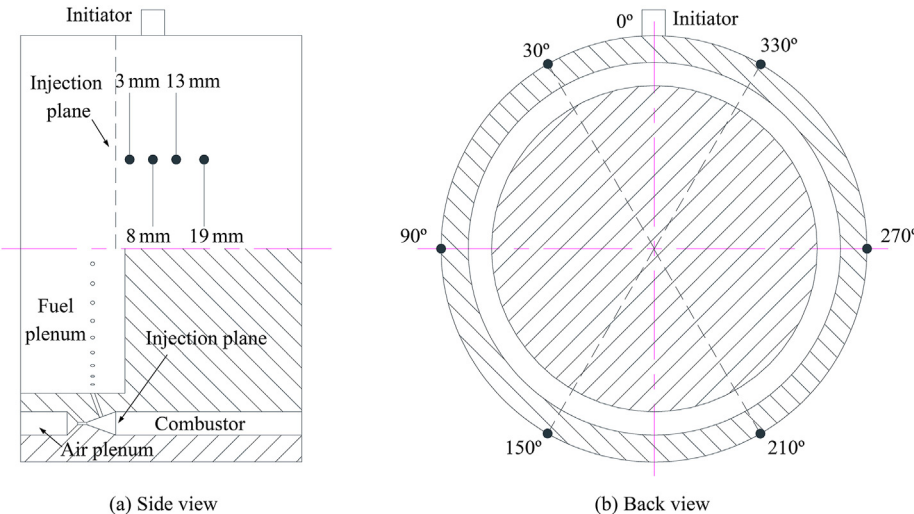


Figure 2 Schematic diagram of injection configuration and instrumentations.

	0°	30°	90°	150°	210°	270°	330°
3/mm			I1		I2		
8/mm	Ignition	I3		PCB1			
13/mm					I4		
19/mm				PCB2			

	0°	30°	90°	150°	210°	270°	330°
3/mm				I3			
8/mm	Ignition	I4		I1			
13/mm					I2		
19/mm			ITP				

respectively. The resonant frequency of this kind of PCB is larger than 500 kHz and the rise time is less than 1 μ s. Average static pressures in the hydrogen and air plenums are measured with the diffused silicon pressure transmitters with sensitivity of 0.5%FS. NI X series multifunction DAQ with data acquisition card (USB-6366) based on NI-STC3 synchronization technology is used to capture the pressure and ionization signals. The frequency of acquisition is 500 kHz, and the operation time of short-duration and long-duration test are set to 0.2 s and 2.2 s, respectively.

The mass flow rates of propellants are regulated by the pressure upstream of the sonic nozzles. The ambient temperature is 298.15 ± 5 K during the tests. The uncertainties in pressure and temperature upstream of the sonic nozzles are ± 0.30 bar and ± 5.0 K, respectively, and the uncertainty in the determination of mass flow rates is analyzed through linearized systematic error. Thus, for the air and hydrogen mass fluxes of $160 \text{ kg}/(\text{m}^2 \cdot \text{s})$ and $7.47 \text{ kg}/(\text{m}^2 \cdot \text{s})$, the uncertainties are $\pm 1.69 \text{ kg}/(\text{m}^2 \cdot \text{s})$ and $\pm 0.11 \text{ kg}/(\text{m}^2 \cdot \text{s})$, respectively, which in turn results in an error of ± 0.029 at the equivalence ratio of 1.60.

3. Results and discussion

The effect of high-pressure detonation products on fuel injection and propagation characteristics of detonation wave was investigated by varying the equivalence ratio, air mass flux, and operation duration. **Table 3** lists the operating conditions during the tests. Frequency is the result of FFT (fast Fourier transform). By varying the equivalence ratio and air mass flux, different propagation frequencies and operation modes of RDW are obtained in the combustor. For the case of equal equivalence ratio, propagation frequency increases with the increase of air mass flux. As shown in the earlier researches, frequency of two steady co-rotating waves is much higher than that of single wave.

Table 3 Operating conditions during the tests.

Test No.	Operation duration/s	Air mass flux/ $(\text{kg}/(\text{m}^2 \cdot \text{s}))$	Equivalence ratio	Frequency/Hz	Operation mode
#1	0.2	108.8	0.83	5560.1	Single wave
#2	0.2	108.8	1.30	6637.0	Single wave
#3	0.2	108.8	1.90	7191.3	Single wave
#4	0.2	63.0	1.54	5662.3	Single wave
#5	0.2	108.8	1.54	7006.0	Single wave
#6	0.2	154.9	1.50	7306.4	Single wave
#7	0.2	167.0	1.60	5184.7/ 12860.7	Longitudinal pulsed detonation
#8	0.2	225.4	1.42	14243.0	Two co-rotating waves
#9	2.2	160.0	1.37	7283.2	Single wave
#10	2.2	160.0	1.60	7446.3	Single wave
#11	2.2	160.0	1.90	7229.4	Single wave
#12	2.2	134.0	1.60	7056.2	Single wave
#13	2.2	203.0	1.60	7600.3	Single wave

Longitudinal pulsed detonation mode is obtained in the combustor when high blockage ratio is set at combustor exit. Short-duration and long-duration tests are performed to investigate the interaction between the combustor and hydrogen plenum, and propagation characteristics of detonation wave in the form of ion voltage.

3.1. The evolution of ion concentration

The detonation wave from the pre-detonator undergoes the process of decoupling and reestablishment after entering the annular combustor, and finally forms a rotating detonation wave propagating continuously in the combustor. There are two typical operation modes including the tangential detonation mode and longitudinal pulsed detonation mode in the rotating detonation combustor depending on the injection configuration and backpressure, which are depicted in [Figures 3 and 4](#), respectively. The main difference between these two modes is the propagation direction of detonation wave. As the name implies, the tangential detonation wave propagates in circumferential direction, and the longitudinal pulsed detonation wave propagates in axial direction in the combustor. Moreover, the longitudinal pulsed detonation wave undergoes periodic decoupling and reestablishment during the test. The time-dependent pressure shown in [Figure 3\(a\)](#) indicates that the development of detonation wave is relatively fast when the tangential detonation occurs in the combustor. [Figure 3\(b\)](#) shows the local pressure signals during the steady period. The propagation frequency of RDW is 7191.3 Hz. Based on the propagation frequency and direction, it is concluded that a single detonation wave exists and propagates circumferentially in the combustor. However, a short period of acoustically-coupled combustion exists in the combustor before the establishment of detonation wave in the

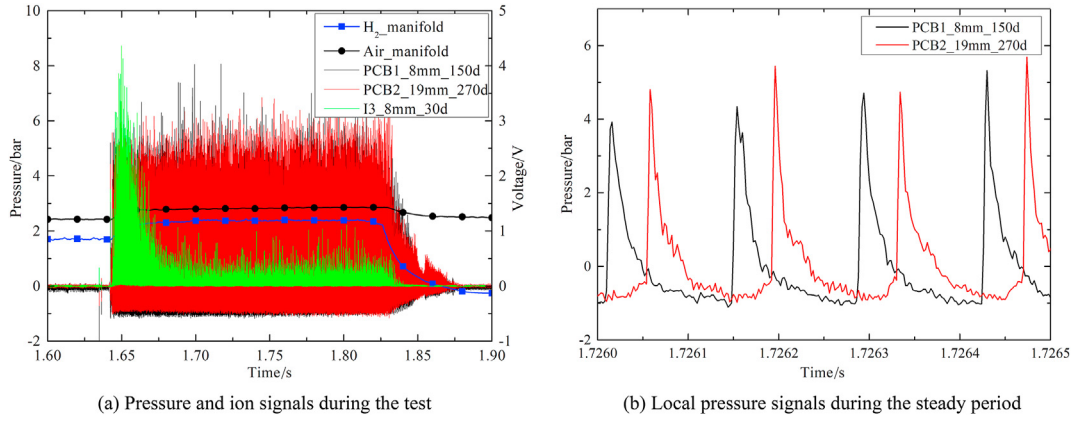


Figure 3 Results of tangential detonation mode ($108.8 \text{ kg}/(\text{m}^2 \cdot \text{s})$, $ER = 1.90$).

longitudinal pulsed detonation mode. Figure 4(b) shows the local pressure signals in the period of acoustically-coupled combustion. The pressure signals at different circumferential locations appear sequentially along the clockwise direction. The propagation frequency during the acoustically-coupled combustion period is 5184.7 Hz. The local pressure signals in the period of longitudinal pulsed detonation are shown in Figure 4(c), two consecutive pressure spikes are observed in the pressure signals in every cycle. Moreover, the time difference between those two pressure spikes depends on the axial location of transducer. Considering the propagation direction and pressure fluctuation values along the axial distance, it is inferred that longitudinal pulsed detonation occurs in the combustor. The frequency of longitudinal pulsed detonation wave is 12860.7 Hz. It is seen that the average pressure in the air and hydrogen plenums will increase after the establishment of detonation wave in the combustor, which is irrelevant to the propagation direction of detonation wave. The most prominent feature is the variation of ion signals, which rise sharply due to the occurrence of detonation, and then decay gradually to a low value state. It should be noted that the low value state is referred as the trough state in the paper.

3.2. Short-duration test

3.2.1. Effect of equivalence ratio

The attenuation of ion voltage implies the decrease of ion concentration in the reaction zone, and it is inferred that the mixture composition in front of the detonation wave must have changed. The lower pressure in the hydrogen plenum compared to that in the air plenum makes the hydrogen plenum suffer more effect of the feedback of high-pressure detonation products. Thus, the average pressure in the hydrogen plenum is selected for analysis. Figure 5 shows the variation of ion voltage and average pressure in the hydrogen plenum with different equivalence ratios when the air mass flux is $108.8 \text{ kg}/(\text{m}^2 \cdot \text{s})$. It is found that the variation of equivalence ratio does not prevent the attenuation of ion voltage. However, the rate for ion voltage decaying to the trough state and the corresponding peak value of ion voltage

are closely related to the equivalence ratio. Increasing the equivalence ratio from 0.83 to 1.30, the peak value of ion voltage increases, and the time for ion voltage decaying to its trough state decreases. Further increasing the equivalence ratio to 1.90 results in a shorter decay time, and the peak value of ion voltage in the trough state decreases slightly. It is seen from Figure 5(a)–(c) that the time for ion voltage decaying to the trough state coincides with the time for the average pressure in the hydrogen plenum reaching its steady state. It is inferred that the attenuation of ion concentration is closely related to the variation of average pressure in the hydrogen plenum. Therefore, it is reasonable to adopt the average pressure in the hydrogen plenum for analysis.

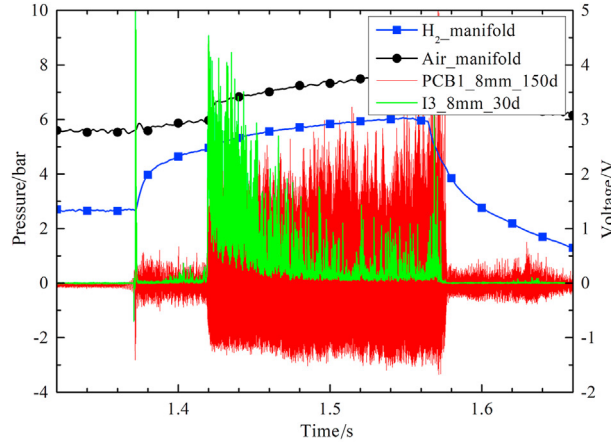
3.2.2. Effect of air mass flux

Figure 6 shows the ion signals and the average pressure in the hydrogen plenum with different air mass fluxes at the equivalence ratio of around 1.50. It is found that the attenuation of ion voltage still exists during the test. The peak value of ion voltage increases first and then decreases at the air mass fluxes ranging from $63.0 \text{ kg}/(\text{m}^2 \cdot \text{s})$ to $154.9 \text{ kg}/(\text{m}^2 \cdot \text{s})$. Comparing to the results in Figure 5, it is evident that the variation of ion voltage with air mass flux has a similar trend to that of equivalence ratio. This is due to the existence of a well-mixed range for equivalence ratio and air mass flux with non-premixed injection of reactants, in which the detonation wave propagates stably, and sufficient ions are produced in the reaction zone. It is seen from Figure 6(a)–(c) that the time for ion voltage decaying to the trough state decreases with the increase of air mass flux.

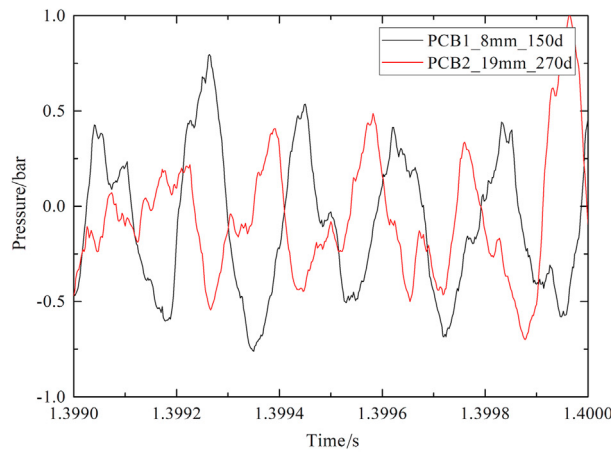
3.2.3. Effect of operation mode

The results from Figures 5 and 6 have revealed that the variation of equivalence ratio and air mass flux do not prevent the attenuation of ion voltage. However, the decay rate and corresponding peak value in the trough state are closely related to those two parameters. Figure 7(a) and (c) show the ion signals and the average pressure in the hydrogen plenum under the two co-rotating waves mode and the longitudinal pulsed detonation mode, respectively. Comparing to the single wave mode, the two co-rotating

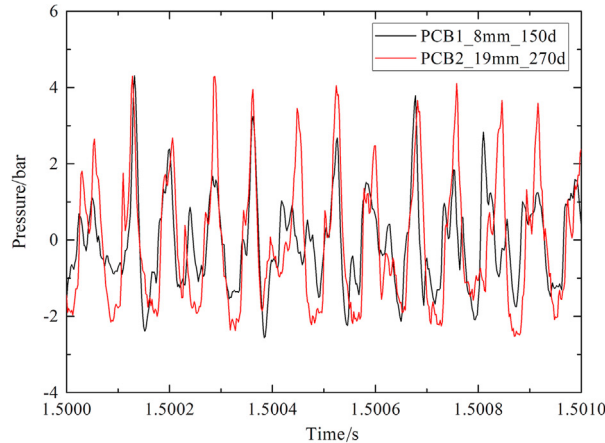
waves mode can be obtained by increasing the air mass flow rate [4,5,8] or blockage ratio at the exit [15]. Therefore, the overall performance of ion signals is similar to that of single wave mode. The local pressure signals under the two co-rotating waves mode are shown in Figure 7(b). The



(a) Pressure and ion signals during the test



(b) Acoustically-coupled combustion period



(c) Longitudinal pulsed detonation period

Figure 4 Results of longitudinal pulsed detonation mode ($167.0 \text{ kg}/(\text{m}^2 \cdot \text{s})$, $ER = 1.60$).

propagation frequency of two co-rotating detonation waves is 14243.0 Hz. Due to the increase of frequency of RDW and average pressure in the hydrogen plenum, the initial peak value and decay rate of ion voltage increase. For the case of longitudinal pulsed detonation, it is seen in

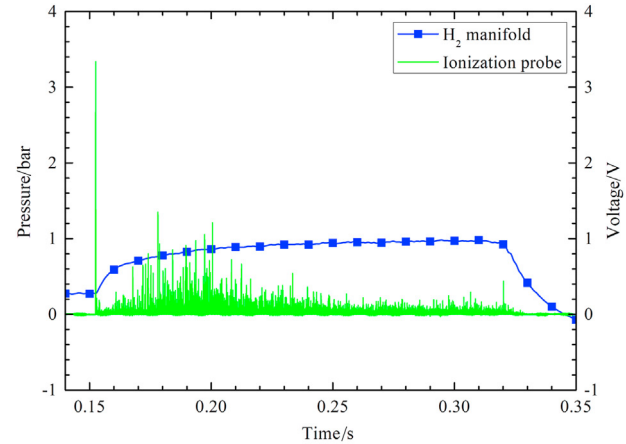
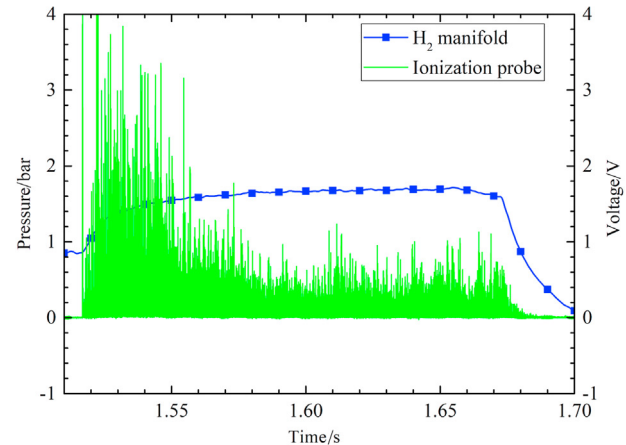
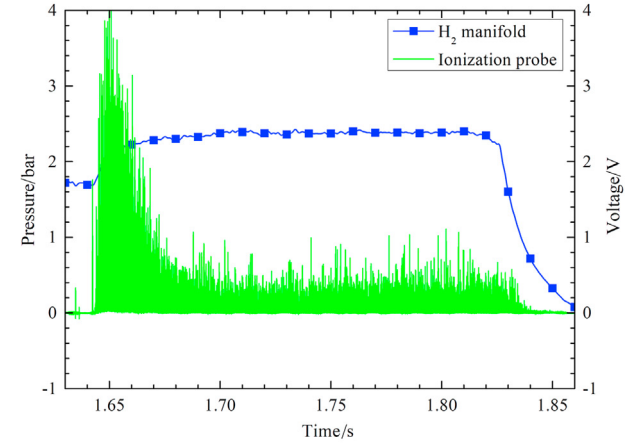
(a) $108.8 \text{ kg}/(\text{m}^2 \cdot \text{s})$, $ER=0.83$ (b) $108.8 \text{ kg}/(\text{m}^2 \cdot \text{s})$, $ER=1.30$ (c) $108.8 \text{ kg}/(\text{m}^2 \cdot \text{s})$, $ER=1.90$

Figure 5 Ion and pressure signals as a function of time for different equivalence ratios at the air mass flux of $108.8 \text{ kg}/(\text{m}^2 \cdot \text{s})$.

Figure 7(c) that the average pressure in the hydrogen plenum increases during the initial acoustically-coupled combustion, however, the ion voltage value is relatively low. This is due to the fact of that the ion concentration in static flame is much lower than that in detonation [29]. Moreover, **Figure 7(c)** shows that the average pressure in the

hydrogen plenum increases during the longitudinal pulsed detonation period, while the ion voltage presents the reverse trend. This phenomenon once again indicates that the attenuation of ion voltage is closely related to the average pressure in the hydrogen plenum.

3.2.4. Analysis of the ion and pressure signals

It has been shown from **Figures 5–7** that the attenuation of ion voltage is general during the initiation of RDW.

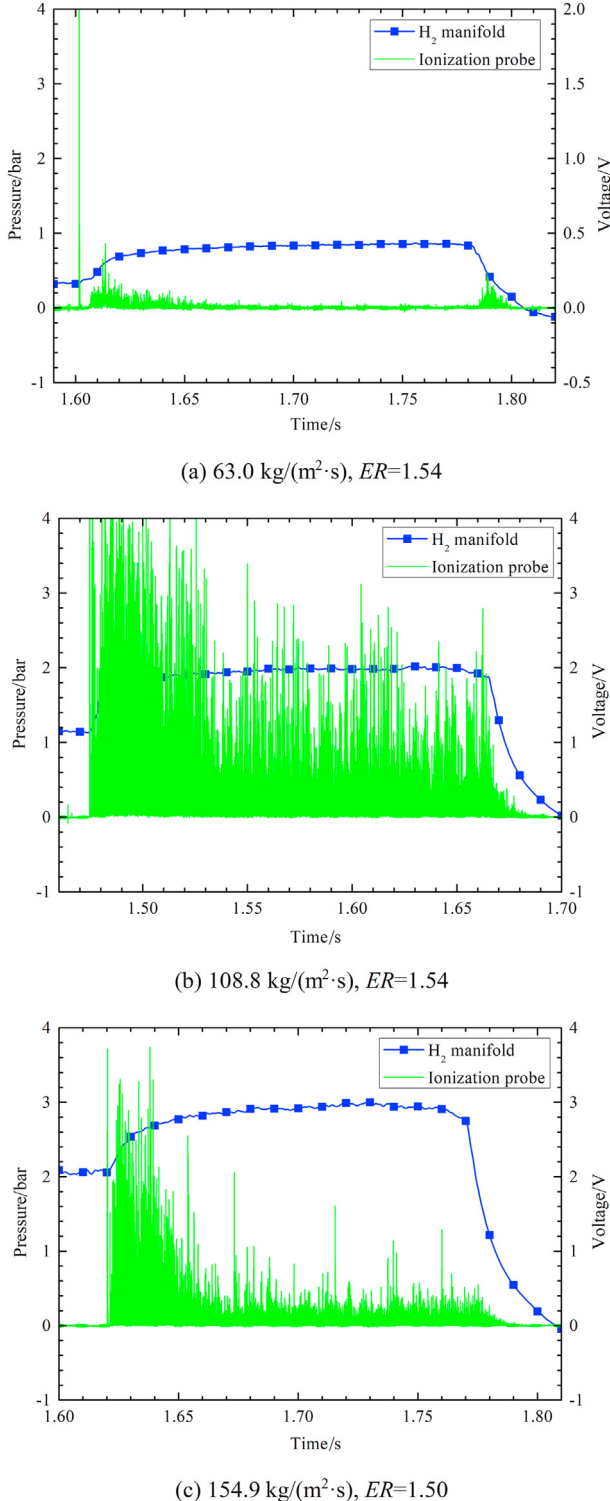


Figure 6 Ion and pressure signals as a function of time for different air mass fluxes at the ER of around 1.5.

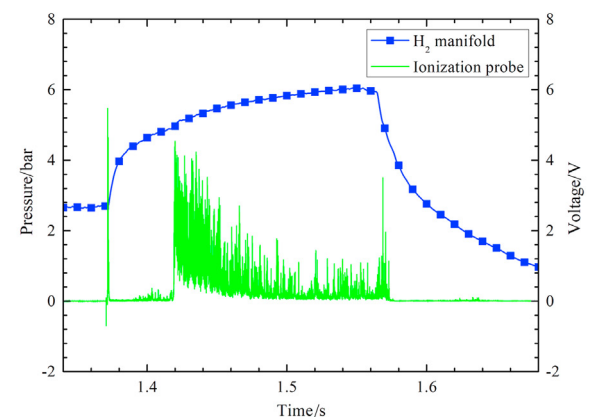
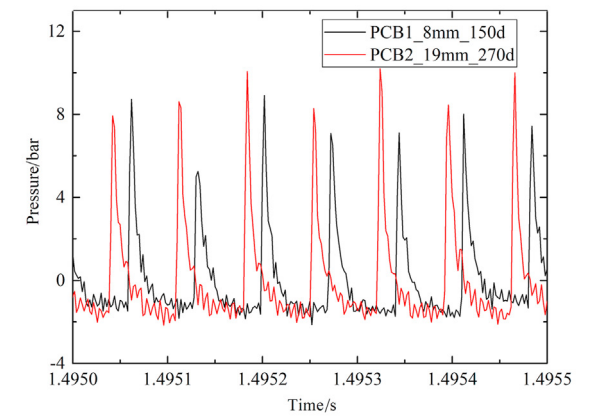
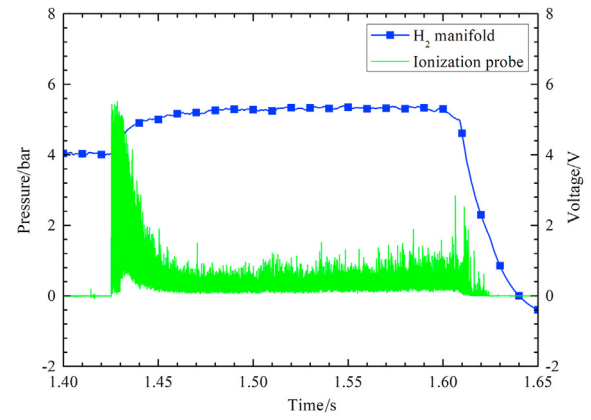


Figure 7 Ion and pressure signals under different operation modes.

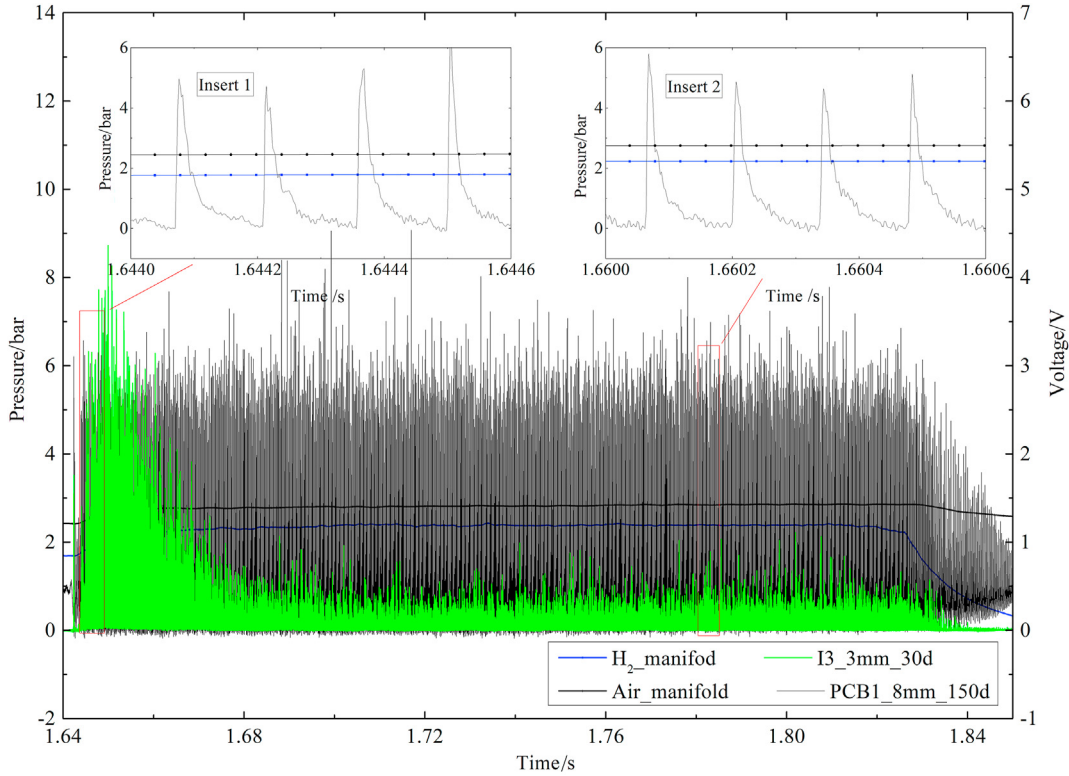


Figure 8 Pressure and ion signals during the test ($108.8 \text{ kg}/(\text{m}^2 \cdot \text{s})$, $ER = 1.90$).

Figure 8 is the local ion and pressure signals during the initial stage of RDW. It is seen that the average pressure in the hydrogen and air plenums increase gradually after the establishment of detonation wave in the combustor. The insert 1 in **Figure 8** shows that the average pressure in the plenums during the initial stage is relatively lower than that in insert 2, which leads to a longer blocked duration (duration of reactant injection occlusion by RDW) for reactant injections. The insert 2 in **Figure 8** shows that the blocked duration for reactant injections decreases when the average pressure in the plenums reaches steady state.

The interaction between the combustor and hydrogen plenum in terms of blockage ratio is shown in **Figure 9**. The

method to calculate the injection blockage ratio is shown in **Figure 9(a)**. It can be seen obviously that the high-pressure detonation products prevent the injection of hydrogen when the instantaneous pressure in the combustor is higher than that in the hydrogen plenum. The injection of hydrogen recovers until the local pressure in the combustor decays to a value lower than the pressure in the hydrogen plenum due to the expansion of detonation products. The parameter t in **Figure 9(a)** represents the period of detonation wave, while t_1 is the blocked duration of hydrogen injection. The blockage ratio is defined as $BR = t_1/t$. **Figure 9(b)** shows the variation of the average pressure in the hydrogen plenum and the blockage ratio during the test. It is found that the

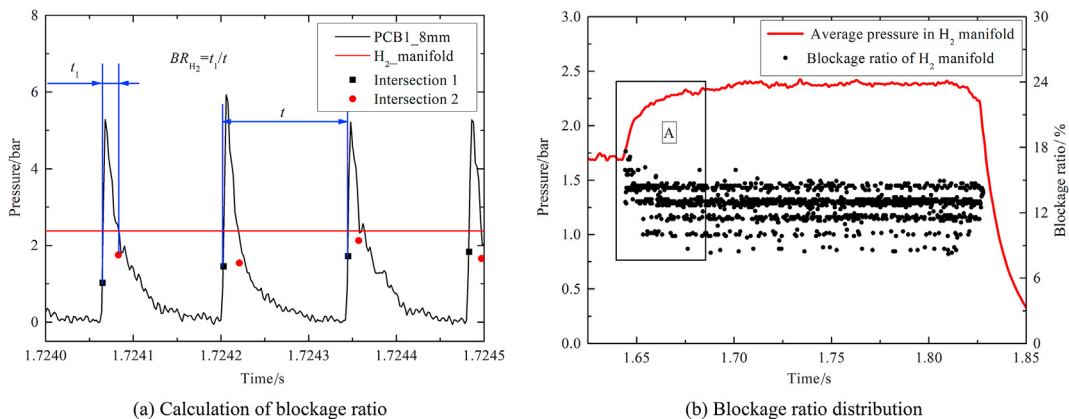


Figure 9 Interaction between the combustor and hydrogen plenum in terms of blockage ratio ($108.8 \text{ kg}/(\text{m}^2 \cdot \text{s})$, $ER = 1.90$).

blockage ratio of hydrogen injection decreases from 18% to 13% in the zone A and remains constant gradually in the rest of test. The decrease of blockage ratio during the initial stage is due to the increase of average pressure in the hydrogen plenum, which is caused by the feedback of high-pressure detonation products. Moreover, the average pressure in the hydrogen plenum and the blockage ratio shown in Figure 9(b) reaches a steady state at around 1.68 s, which is coincident with the time that the ion voltage reaches the trough state in Figure 8. This coincidence demonstrates that the attenuation of ion voltage is determined by the pressure behavior in the hydrogen plenum. It is inferred that the feedback of high-pressure detonation products into the hydrogen plenum causes the decrease of fuel concentration in front of RDW, resulting in the attenuation of ion voltage in the reaction zone during the initial stage of RDW.

It is seen in Figure 8 that the pressure rise across RDW has negligible change during the attenuation stage of ion voltage. Considering the relationship between detonation strength and propagation velocity, the velocity-time distribution of RDW is obtained, as shown in Figure 10. The instantaneous velocity during the test is relatively stable despite of some little variations. The local velocity-time distribution during the attenuation stage and the subsequent trough stage of ion voltage are shown in the insert 1 and insert 2, respectively. The propagation velocity of RDW in the initial stage (1.643–1.655 s) is slightly lower than that in the trough stage, and the instantaneous velocity remains almost constant after 1.655 s. It is found that the

feedback of high-pressure detonation products has slight effect on the pressure rise across RDW and detonation velocity during the attenuation stage of ion voltage. This seems to be contrary to the classical detonation theory that the detonation velocity and pressure rise only depend on the state of reactants before RDW. The inconsistency could be due to the highly inhomogeneous mixing of fresh reactants. The non-ideal spatial distribution of fuel in the reactants leads to highly irregular structure of RDW [4], which in turn results in the existence of unburned gas pocket after the sonic surface. Thus, only part of energy is contributed to the propagation of RDW. However, the contact of high-temperature detonation products increases the temperature of fresh reactants, which reduces the amount of unburned gas pockets before the sonic surface. Moreover, sonic speed and specific heat ratio of the reactants are changed due to the interaction between the fresh reactants and the high-temperature products. Besides above factors, the RDE geometry will also result in a detonation that strays from one-dimensional ZND theory. In summary, the detonation velocity and the pressure rise across RDW suffer little effect from the feedback of high-pressure detonation products.

3.3. Long-duration test

The results from short-duration tests indicate that the ion voltage decays gradually from the initial high value to a low value of the trough state. It seems that the interaction between the combustor and hydrogen plenum reaches a steady

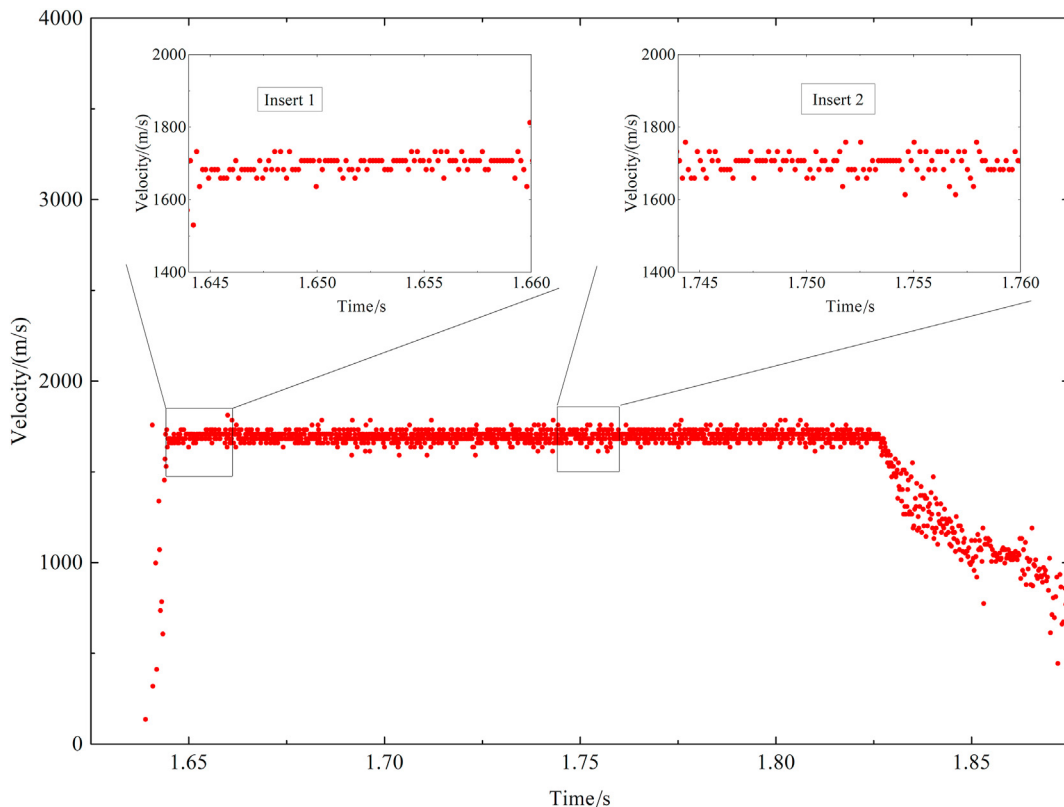


Figure 10 Velocity-time distribution.

state. However, it is unknown whether the ion concentration will change with the increase of test duration. Thus, long-duration tests are carried out to further investigate the trend of ion concentration. The results of long-duration test are shown in Figure 11.

Figure 11(a) shows the static pressure in the combustor and plenums during the test. It is found that the average pressure in the combustor and plenums increases after the establishment of detonation wave in the combustor. The static pressure in the combustor and hydrogen plenum remains constant after a short period of development, while the static pressure in the air plenum increases during the whole test. This could be due to the fact of that the injection area of air is much larger than that of hydrogen, which leads to the easier feedback of leading shock wave into the air plenum. Moreover, the volume of air plenum (75987.3 mm^3) is much smaller than that of hydrogen plenum (190262.8 mm^3). It is more difficult for the air plenum to dissipate the shock wave induced by detonation wave from the combustor, and the continuous reflection of shock wave results in a longer time for the air plenum to reach a steady state [10]. Figure 11(b) shows the time-dependent dynamic pressure measured by ITP measurement, which reveals the continuous propagation of RDW in the combustor, without the occurrence of significant flameout. The insert in Figure 11(b) shows the local pressure during the test. Although the practical peak pressure is difficult to be obtained from the insert, it provides the exact operation frequency of detonation wave. The short-time Fourier transform result based on the time-dependent dynamic pressure data is shown in Figure 11(c), which indicates a stable propagation of RDW in the whole test.

3.3.1. Effect of equivalence ratio

The static pressure in the hydrogen plenum remains constant during the long-duration test, as shown in Figure 11(a), which indicates that the pressure equilibrium between the hydrogen plenum and combustor has been established. Figure 9(a) shows that the feedback and purgation of high-pressure detonation products in the hydrogen plenum is a dynamic process. When the purgation of high-pressure detonation products is greater than the feedback of high-pressure detonation products, the concentration of fuel in the reactants increases, and the ion voltage measured by ion probe will recover to a steady state. Figures 12–14 show the trend of ion voltage and corresponding short-time Fourier transform result with different equivalence ratios at the air mass fluxes of $160 \text{ kg}/(\text{m}^2 \cdot \text{s})$.

It has been shown in Figures 12(a)–14(a) that the ion voltage recovers to a steady state gradually after the trough stage during the long-duration test. Although the static pressure in the hydrogen plenum remains constant during the test, the balance between the hydrogen injection and feedback of high-pressure detonation products has not reach the steady state. The feedback of detonation products into the hydrogen plenum leads to the initial attenuation of ion voltage, and then the purgation of detonation products is

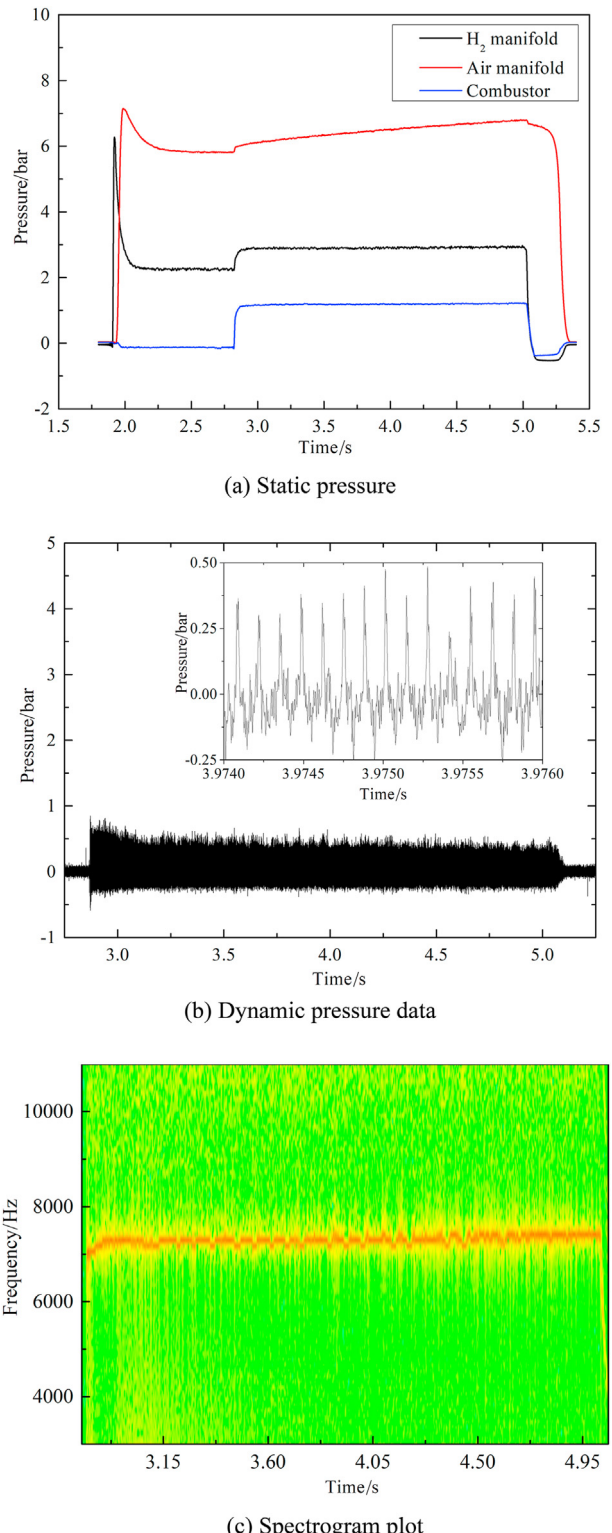


Figure 11 Results at the air mass flux of $160 \text{ kg}/(\text{m}^2 \cdot \text{s})$, $ER = 1.37$.

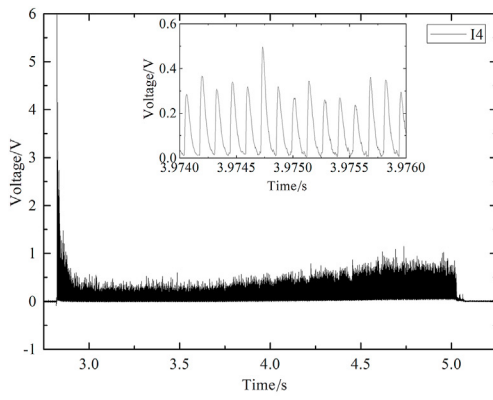
greater than the feedback of detonation products, which results in the gradual recovery of ion voltage.

The trend of ion voltage from Figures 12(a)–14(a) reveals that the recovery rate of ion voltage and corresponding peak value of the steady state are closely related to the equivalence ratio. For the case of $ER = 1.37$, the ion

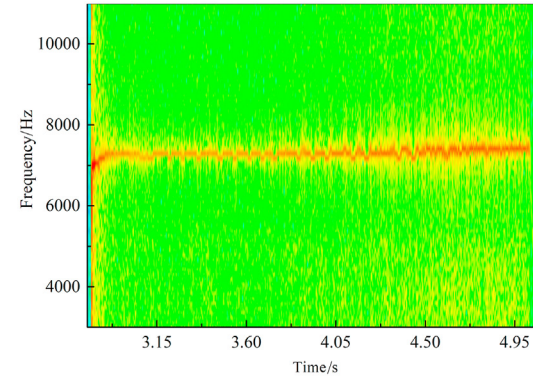
voltage starts to rise at 3.75 s and reaches the steady state at around 4.75 s, and the corresponding peak value is about 0.80 V. Increasing the equivalence ratio to 1.60, the ion voltage starts to rise at 3.17 s and recovers to a steady value of 1.5 V at around 3.86 s. Further increasing the equivalence ratio to 1.90, the ion voltage starts to increase at around 3.1 s, and reaches a steady value of 2 V at around 4.0 s. Considering the results from Figure 5, it is found that the

decay rate and recovery rate of ion voltage increase with the increase of equivalence ratio, and the recovery of ion voltage starts earlier at the higher equivalence ratio. In addition, the increase of equivalence ratio leads to the increase of peak value of ion voltage under the steady state.

Figures 12(b)–14(b) show the short-time Fourier transform results of corresponding ion signals in Figures 12(a)–14(a). It can be found that the instantaneous frequency of

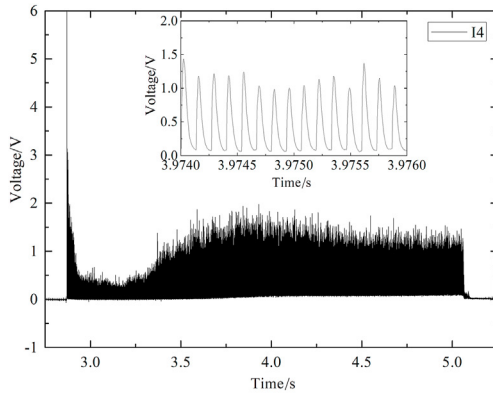


(a) Evolution of ion voltage

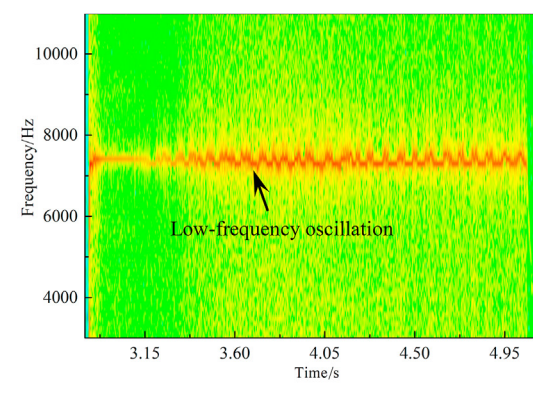


(b) Spectrogram plot

Figure 12 Results at the air mass flux of $160 \text{ kg}/(\text{m}^2 \cdot \text{s})$, $ER = 1.37$.

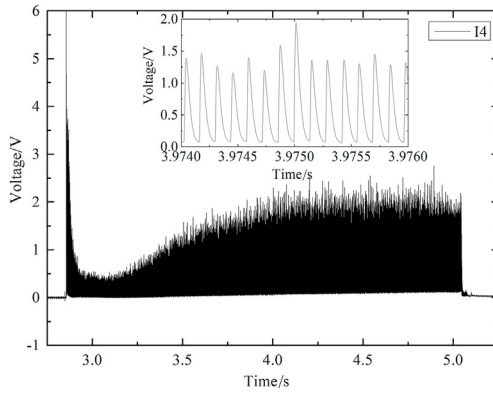


(a) Evolution of ion voltage

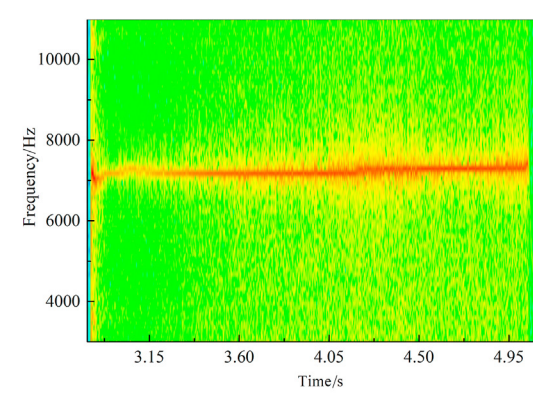


(b) Spectrogram plot

Figure 13 Results at the air mass flux of $160 \text{ kg}/(\text{m}^2 \cdot \text{s})$, $ER = 1.60$.



(a) Evolution of ion voltage



(b) Spectrogram plot

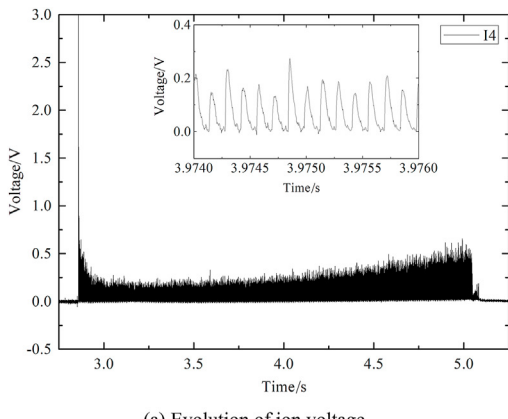
Figure 14 Results at the air mass flux of $160 \text{ kg}/(\text{m}^2 \cdot \text{s})$, $ER = 1.90$.

RDW remains almost constant before the steady state and increases slightly during the steady state at the equivalence ratio of 1.37. Moreover, the short-time Fourier transform result shows that a low-frequency oscillation occurs at around 0.25 s after the establishment of RDW in the combustor, which is presented as the fluctuation of frequency in Figure 12(b). Increasing the equivalence ratio to 1.60, the instantaneous frequency remains constant during the initial 0.3 s, which corresponds to the attenuation stage and trough stage of ion voltage, as shown in Figure 13(a). A regular low-frequency oscillation occurs in the instantaneous frequency when the ion voltage starts to recover. Comparing to the short-time Fourier transform result in Figure 12(b), the low-frequency oscillation is more obvious. Further increasing the equivalence ratio to 1.90, the short-time Fourier transform result shown in Figure 14(b) exhibits a slight rise in the instantaneous frequency during the initial 0.25 s. However, the operation frequency remains constant during the subsequent 0.9 s, which corresponds to the recovery period of ion voltage (3.1–4.0 s). In addition, the instantaneous frequency increases slightly when the ion voltage reaches the steady state. The most significant difference in Figures 12(b)–14(b) is the absence of low-frequency oscillation in the instantaneous frequency in

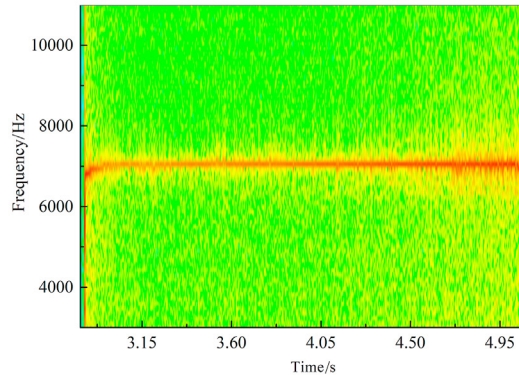
Figure 14(b). It is inferred that the purgation of detonation products has limited effect on the instantaneous frequency of RDW. When the equivalence ratio is lower than 1.60, the low-frequency oscillation occurs and its starting time coincides with the recovery time of ion voltage.

3.3.2. Effect of air mass flux

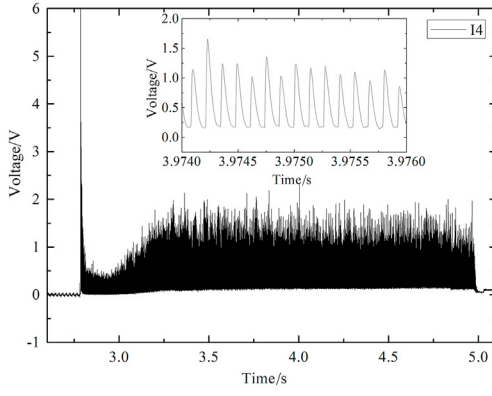
It has been shown in Figure 6 that the air mass flux has important effect on the decay rate of ion voltage during the attenuation stage. Based on Figure 6 results, air mass flux may also have an impact on ion voltage recovery rate and peak value of steady state. Figure 15 and Figure 16 show the ion voltage signals and corresponding short-time Fourier transform results at the air mass flux of $134 \text{ kg}/(\text{m}^2 \cdot \text{s})$ and $203 \text{ kg}/(\text{m}^2 \cdot \text{s})$, respectively. The global equivalence ratio is 1.60 during the tests of various air mass fluxes. For the air mass flux of $134 \text{ kg}/(\text{m}^2 \cdot \text{s})$ shown in Figure 15, the ion voltage starts to rise at around 3.5 s, however, the low recovery rate leads to the difficulty to determine whether the ion voltage reaches the steady state at the end of test. Moreover, the peak value of ion voltage at the end of test is only 0.5 V, which is relatively low. Increasing the air mass flux to $203 \text{ kg}/(\text{m}^2 \cdot \text{s})$, the ion voltage starts to increase at 2.85 s and reaches a steady value of 1.7 V at around 3.25 s.



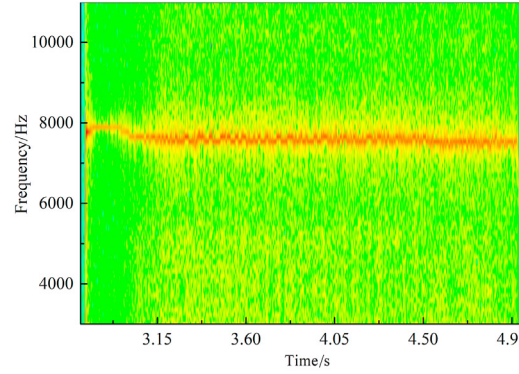
(a) Evolution of ion voltage



(b) Spectrogram plot

Figure 15 Results at the air mass flux of $134 \text{ kg}/(\text{m}^2 \cdot \text{s})$, $ER = 1.60$.

(a) Evolution of ion voltage



(b) Spectrogram plot

Figure 16 Results at the air mass flux of $203 \text{ kg}/(\text{m}^2 \cdot \text{s})$, $ER = 1.60$.

Comparing to the results shown in Figure 13, it is found that the recovery rate of ion voltage increases with the increase of air mass flux, and the recovery of ion voltage starts earlier at the higher air mass flux. Moreover, the peak value of ion voltage in the steady state also increases with the increase of air mass flux.

Figures 15(b) and 16(b) represent the short-time Fourier transform result based on ion voltage signals at the air mass fluxes of $134 \text{ kg}/(\text{m}^2 \cdot \text{s})$ and $203 \text{ kg}/(\text{m}^2 \cdot \text{s})$, respectively. Figure 15(b) shows that the instantaneous operation frequency is almost constant, and the low-frequency oscillation is not observed during the whole test. However, the short-

time Fourier transform result at the air mass flux of $160 \text{ kg}/(\text{m}^2 \cdot \text{s})$ exhibits a significant low-frequency oscillation in the RDW, as shown in Figure 13(b). For the air mass flux of $203 \text{ kg}/(\text{m}^2 \cdot \text{s})$, the instantaneous frequency of RDW shows a slight low-frequency oscillation during the recovery of ion voltage, as shown in Figure 16(b). The operation frequency remains constant about 8000 Hz during the initial 0.2 s after the establishment of RDW, which corresponds to the attenuation stage and trough stage of ion voltage. The instantaneous frequency exhibits a decrease with the recovery of ion voltage, and the low-frequency oscillation occurs in the RDW at the same time.

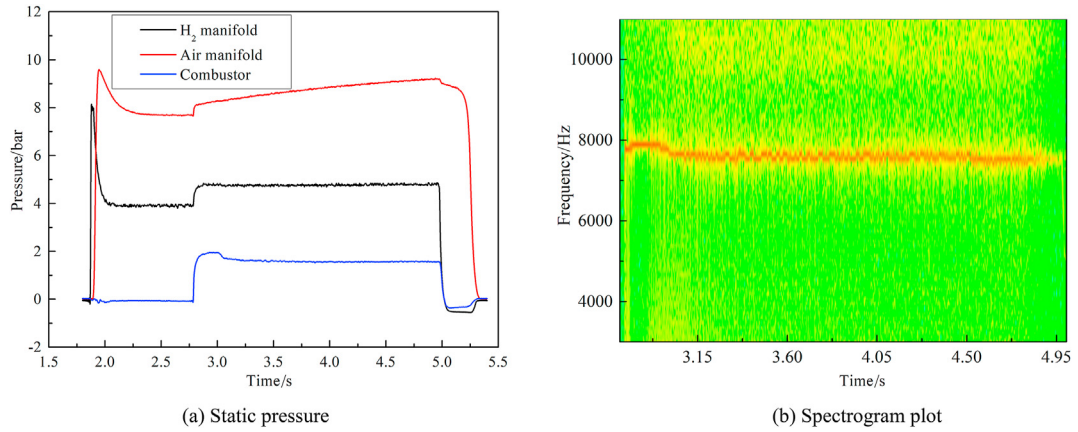


Figure 17 Results at the air mass flux of $203 \text{ kg}/(\text{m}^2 \cdot \text{s})$, $ER = 1.60$.

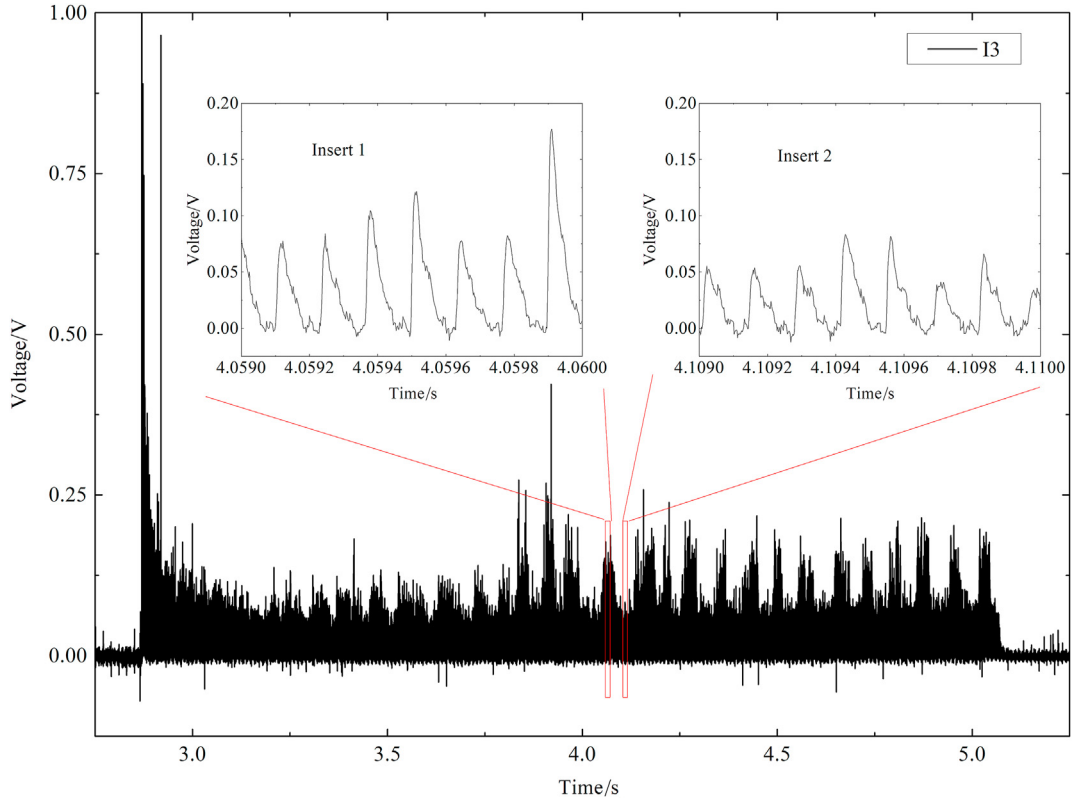


Figure 18 Ion signals at the air mass flux of $160 \text{ kg}/(\text{m}^2 \cdot \text{s})$, $ER = 1.60$.

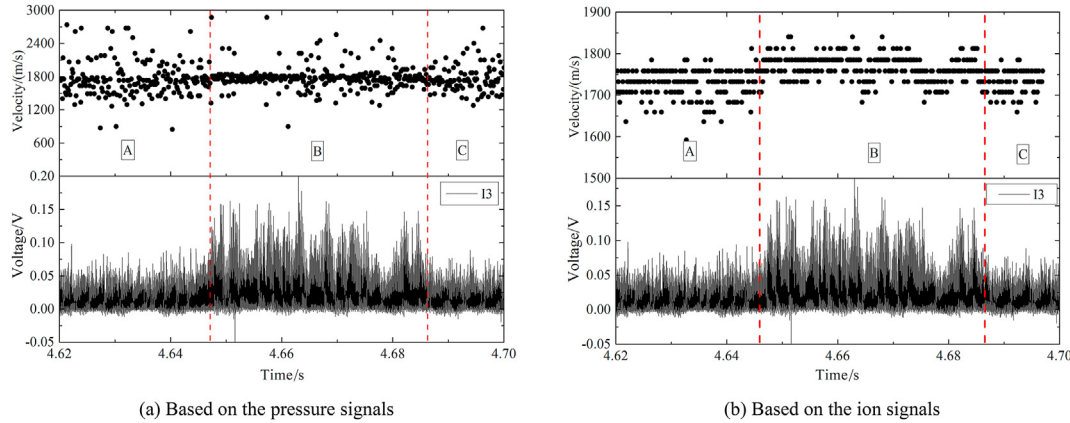


Figure 19 Analysis of instantaneous velocity.

A different feature in Figure 16(b) is the occurrence of a decrease of instantaneous frequency before the recovery of ion voltage. The corresponding static pressure in the combustor and plenums and the short-time Fourier transform result of pressure signals acquired by ITP are shown in Figure 17. It can be seen that the fluctuation of instantaneous frequency of RDW almost has no effect on the average pressure in the air and hydrogen plenums. Differently, the average pressure in the combustor is closely related to the operation frequency. It is clearly seen that the static pressure in the combustor remains a high value during the period of 2.75 s–3.0 s, which coincides with the duration of higher frequency in Figure 17(b). The static pressure in the combustor drops down when a drop of instantaneous frequency occurs in RDW. This phenomenon could be due to the fact of that a large number of high-temperature detonation products feed back into the hydrogen plenum during the initial stage, which results in the increase of sonic speed in the reactants. Thus, the propagation velocity of RDW increases. When the purgation of detonation products is greater than the feedback of detonation products, the ion voltage starts to recover, and the sonic speed in the fresh reactants decreases, which leads to a drop of instantaneous frequency.

3.4. Low-frequency oscillation

The most significant phenomenon in the short-time Fourier transform results is the low-frequency oscillation, as shown in Figures 12(b), 13(b) and 16(b). Figure 18 shows the ion voltage signal detected by I3, which is located at 3 mm downstream of the injection plane. Comparing with the results in Figure 13, the peak value of ion voltage detected by I3 is much lower than that detected by I4 (8 mm downstream of the injection plane). It could be due to the presence of an inhomogeneous mixing zone near the head of the combustor, which results in some low activity mixtures at 3 mm. The mixing degree of H₂ and air increases with the increase of axial distance [30], which guarantees a stronger detonation wave and more ions in the post-detonation zone. As shown in Figure 18, it is clearly found that the low-frequency oscillation occurs at around 3.2 s, at which the

ion voltage starts to recover. The insert 1 and insert 2 in Figure 18 show the local view of ion signals in the peak and trough of low-frequency oscillation, respectively. There are many burrs existing in the ion signals, which indicate the existence of fluctuations in the reaction zone. Some of the reactants complete the energy release through turbulent combustion.

Figure 19(a) and (b) show the velocity-time distributions based on the time-dependent pressure and ion signals during 4.62 s–4.7 s, respectively. It is seen in Figure 19(a) that the instantaneous velocities are convergent in peak zone B, while the instantaneous velocities are dispersed in trough regions A and C. Figure 19(b) shows that the instantaneous velocities in trough regions A and C are slightly lower than those in peak region B. Thus, it is inferred that the low-frequency oscillation has a certain influence on the instantaneous velocity of RDW.

From the short-time Fourier transform results shown in Figures 12–17, it is found that the low-frequency oscillation occurs at the time that the ion voltage starts to recover. The frequency of the low-frequency oscillation is 10–12 Hz, which is far lower than the low-frequency sinusoidal oscillation (around 200 Hz) observed in many experiments [31]. The common low-frequency sinusoidal oscillation can be suppressed by increasing the injection pressure of reactants. However, there is no significant relationship between low-frequency oscillation and injection pressure in studies during this research. Table 4 lists the results of low-

Table 4 Results of low-frequency oscillation and corresponding injection pressure ratio.

Equivalence ratio	Air mass flux/(kg/(m ² ·s))	Injection pressure ratio	Low-frequency oscillation/Hz
1.37	160	1.74	10.1
1.60	160	1.99	11.3
1.90	160	2.26	—
1.60	134	1.82	—
1.60	203	2.27	11.9

frequency oscillation and corresponding injection pressure ratio (ratio of average pressure in the hydrogen plenum and combustor) under different conditions. It is seen that the increase of equivalence ratio suppresses this low-frequency oscillation at the constant air mass flux, and the decrease of air mass flux also suppresses this low-frequency oscillation at the constant equivalence ratio. However, the occurrence of this low-frequency oscillation cannot be exactly determined through injection pressure ratio. The increase of injection pressure ratio promotes the occurrence of low-frequency oscillation at some conditions. The occurrence of low-frequency oscillation is closely related to the purgation of detonation products. Thus, it is inferred that the low-frequency oscillation is caused by the coupling between the combustor and hydrogen plenum, and the mechanism of the occurrence of low-frequency oscillation requires further investigation.

4. Conclusions

The effect of high-pressure detonation products on fuel injection and propagation characteristics of detonation wave has been investigated in the form of ion voltage by varying the equivalence ratio, air mass flux, and operation duration with hydrogen-air mixtures. The main conclusions are drawn as follows:

- (1) The attenuation of ion voltage during the initial stage of RDW is a general phenomenon, which is caused by the feedback of high-pressure detonation products into the hydrogen plenum. The increase of equivalence ratio and air mass flux increase the decay rate of ion voltage.
- (2) The balance between the hydrogen injection and feedback of high-pressure detonation products has not been established during the short-duration tests. The feedback and purgation of high-pressure detonation products in the hydrogen plenum is a dynamic process.
- (3) The long-duration tests show that the ion voltage will gradually recover to a steady state after the initial attenuation when the purgation of detonation products is greater than the feedback of detonation products in the hydrogen plenum. The higher equivalence ratio and air mass flux lead to the earlier recovery of ion voltage and higher peak value in the steady state. In addition, the increase of equivalence ratio and air mass flux accelerate the recovery of ion voltage.
- (4) Low-frequency oscillation about 10–12 Hz occurs in the RDW at some operation conditions. It is inferred that this low frequency oscillation is caused by the coupling between the combustor and hydrogen plenum, and can be eliminated by either increasing the equivalence ratio or decreasing the air mass flux. The mechanism of the occurrence of low-frequency oscillation requires further investigation.

Acknowledgement

This work was supported by National Natural Science Foundation of China (12072163, 52106161, 11802134), National Defense Science and Technology Key Laboratory Foundation (HTKJ2020KL011004-1), and China Postdoctoral Science Foundation (2020M681616).

References

- [1] J.H.S. Lee, *The Detonation Phenomenon*, Cambridge University Press, New York, 2008, pp. 73–75.
- [2] P. Wolanski, Detonative propulsion, *Proc. Combust. Inst.* 34 (2013) 125–158.
- [3] A.C. St George, R.B. Driscoll, D.E. Munday, E.J. Gutmark, Development of a rotating detonation engine facility at the University of Cincinnati, in: 53rd AIAA Aerospace Sciences Meeting, Florida, America, 5–9 January 2015.
- [4] B.A. Rankin, D.R. Richardson, A.W. Caswell, A.G. Naples, J.L. Hoke, F.R. Schauer, Chemiluminescence imaging of an optically accessible non-premixed rotating detonation engine, *Combust. Flame* 176 (2017) 12–22.
- [5] W. Lin, J. Zhou, S. Liu, Z. Lin, F. Zhuang, Experimental study on propagation mode of H₂/Air continuously rotating detonation wave, *Int. J. Hydrogen Energy* 40 (4) (2015) 1980–1993.
- [6] C. Yang, X. Wu, H. Ma, L. Peng, J. Gao, Experimental research on initiation characteristics of a rotating detonation engine, *Exp. Therm. Fluid Sci.* 71 (2016) 154–163.
- [7] F.A. Bykovskii, S.A. Zhdan, E.F. Vedernikov, Continuous spin detonation in annular combustors, *Combust. Explos. Shock Waves* 41 (4) (2005) 449–459.
- [8] F.A. Bykovskii, S.A. Zhdan, E.F. Vedernikov, Continuous spin detonations, *J. Propul. Power* 22 (6) (2012) 1204–1216.
- [9] V. Anand, A.S. George, R. Driscoll, E. Gutmark, Investigation of rotating detonation combustor operation with H₂-Air mixtures, *Int. J. Hydrogen Energy* 41 (2) (2016) 1281–1292.
- [10] P.A. Cocks, A.T. Holley, B.A. Rankin, High fidelity simulations of a non-premixed rotating detonation engine, in: 54th AIAA Aerospace Sciences Meeting, California, America, 4–8 January 2016.
- [11] A. Roy, D.H. Ferguson, T. Sidwell, B. O'Meara, P. Strakey, C. Bedick, A. Sisler, Experimental study of rotating detonation combustor performance under preheat and back pressure operation, in: 55th AIAA Aerospace Sciences Meeting, Texas, America, 9–13 January 2017.
- [12] J. Suchocki, S.T. Yu, J. Hoke, A. Naples, F. Schauer, R. Russo, Rotating detonation engine operation, in: 50th AIAA Aerospace Sciences Meeting Including the New Horizons Forum and Aerospace Exposition, Tennessee, America, 9–12 January 2012.
- [13] R. Russo, P. King, F. Schauer, L. Thomas, Characterization of pressure rise across a continuous detonation engine, in: 47th AIAA/ASME/SAE/ASEE Joint Propulsion Conference and Exhibit, California, America, 31 July–3 August 2011.
- [14] F.A. Bykovskii, E.F. Vedernikov, Continuous detonation of a subsonic flow of a propellant, *Combust. Explos. Shock Waves* 39 (3) (2003) 323–334.
- [15] S.M. Frolov, V.S. Aksenov, V.S. Ivanov, I.O. Shamshin, Large-scale hydrogen-air continuous detonation combustor, *Int. J. Hydrogen Energy* 40 (3) (2015) 1616–1623.
- [16] V. Anand, A.S. George, R. Driscoll, E. Gutmark, Longitudinal pulsed detonation instability in a rotating detonation combustor, *Exp. Therm. Fluid Sci.* 77 (2016) 212–225.
- [17] M.L. Fotia, J.L. Hoke, F. Schauer, Propellant Plenum Dynamics in a Two-Dimensional Rotating Detonation Experiment, in: 52nd Aerospace Sciences Meeting, Maryland, America, 13–17 January 2014.

- [18] D.A. Schwer, K. Kailasanath, On reducing feedback pressure in rotating detonation engines, in: 51st AIAA Aerospace Sciences Meeting, Texas, America, 7-10 January 2013.
- [19] V. Anand, A.S. George, R. Driscoll, E. Gutmark, Analysis of air inlet and fuel plenum behavior in a rotating detonation combustor, *Exp. Therm. Fluid Sci.* 70 (2016) 408–416.
- [20] M.L. Fotia, J. Hoke, F. Schauer, Experimental ignition characteristics of a rotating detonation engine under backpressured conditions, in: 53rd AIAA Aerospace Sciences Meeting, Florida, America, 5-9 January 2015.
- [21] A. Naples, J. Hoke, F. Schauer, Rotating detonation engine interaction with an annular ejector, in: 52nd Aerospace Sciences Meeting, Maryland, America, 13–17 January 2014.
- [22] M. Zhao, H. Zhang, Origin and chaotic propagation of multiple rotating detonation waves in hydrogen/air mixtures, *Fuel* 275 (2020) 117986.
- [23] C. Yan, H. Teng, H.D. Ng, Effects of slot injection on detonation wavelet characteristics in a rotating detonation engine, *Acta Astronaut.* 182 (5) (2021) 274–285.
- [24] R. Burke, T. Rezzag, I. Dunn, W. Flores, K. Ahmed, The effect of premixed stratification on the wave dynamics of a rotating detonation combustor, *Int. J. Hydrogen Energy* 46 (2021) 27816–27826.
- [25] T.M. Helfrich, F.R. Schauer, R.P. Bradley, J.L. Hoke, Ignition and detonation-initiation characteristics of hydrogen and hydrocarbon fuels in a PDE, in: 45th AIAA Aerospace Sciences Meeting and Exhibit, Nevada, America, 8-11 January 2007.
- [26] J.S. Zdenek, Ion Based Pressure Sensor for Pulse Detonation Engines, Master Dissertation, Aeronautics and Astronautics Department, Air University, Ohio, March, 2004.
- [27] J. Meredith, H.D. Ng, J.H.S. Lee, Detonation diffraction from an annular channel, *Shock Waves* 20 (6) (2010) 449–455.
- [28] G. Ciccarelli, S. Dorofeev, Flame acceleration and transition to detonation in ducts, *Prog. Energy Combust. Sci.* 34 (4) (2008) 499–550.
- [29] A.J. Laderman, G.J. Hecht, R.A. Stern, A.K. Oppenheim, Flame ionization during the development of detonation, *Symposium (International) on Combustion* 8 (1) (1961) 199–206.
- [30] R. Driscoll, A.S. George, E.J. Gutmark, Numerical investigation of injection within an axisymmetric rotating detonation engine, *Int. J. Hydrogen Energy* 41 (3) (2015) 2052–2063.
- [31] V. Anand, A.S. George, R. Driscoll, E. Gutmark, Characterization of instabilities in a rotating detonation combustor, *Int. J. Hydrogen Energy* 40 (46) (2015) 16649–16659.